
Experimental Tools for Nuclear Astrophysics

C. Angulo

Université catholique de Louvain, Louvain-la-Neuve, Belgium

Abstract This chapter concentrates on experimental techniques currently used to investigate nuclear reactions of astrophysical interest. After a brief introduction, I shall present the basic quantities and equations governing thermonuclear reaction rates in stellar plasma. The various astrophysical scenarios, from hydrostatic to advanced burning stages up to/and including explosive mechanisms, as well as some key reactions, are briefly presented. I will concentrate on the experimental approaches to study nuclear reactions involved in both quiescent and explosive stellar burning. Particular emphasis is given to the use of radioactive ion beams and their importance for characterizing explosive nucleosynthesis in novae and X-ray bursts. A few recent examples will be shown in more detail to illustrate these techniques. Some key open questions will be discussed in the context of future facilities.

1 Understanding the Universe

The present configuration of the Universe is the result of the evolution of the primordial matter which was mainly composed, a few minutes after the Big Bang,¹ of the two lightest elements, hydrogen and helium. It is well-known at present that all other chemical elements, that make up, for instance, all living beings and celestial objects have been produced by nuclear reactions in the heart of stars (see, for example, the review papers on stellar nucleosynthesis [1–5]). These nuclear reactions produce the energy that powers the stars and this balances the gravitational force to prevent their collapse. In turn, the production of energy and elements explain the structure and evolution of the Universe, with stars that will progressively cool down and die and stars that will explode producing cataclysmic events.

To understand the structure and the evolution of the Universe it is essential to understand the synthesis of the elements [6]. Most of the questions about

¹ The theory of the Big Bang established 80 years ago, is largely accepted at present as the theory of the origin of the Universe.

the nucleosynthesis have been answered by nuclear physics in the twentieth century, with remarkable contributions from, among others, H. Bethe [7–9] and F. Hoyle [10]. The reader will find a concise but rather complete historical review in the book of D.D. Clayton [6]. Just 50 years ago, in a famous review article [11], E.M. Burbidge, G.R. Burbidge, W.A. Fowler and F. Hoyle gave a complete explanation of the synthesis of elements by different nuclear mechanisms. They explained hydrogen burning in the Big Bang and in the main sequence stars (such as our sun), helium burning and the triple- α process in red giant stars and in the asymptotic giant branch stars, as well as the production of elements beyond iron by the *s*-process (slow neutron capture reactions), the *r*-process (rapid neutron capture reactions) and the *p*-process (photodisintegration and proton capture reactions).

Modern nuclear astrophysics has thus been born on the crossroad of nuclear physics, astrophysics and astronomy. It involves careful and dedicated experimental and theoretical studies of a large variety of nuclear processes (nuclear physics) as indispensable tools for the modelling of stellar evolution and nucleosynthesis (astrophysics). Nuclear reactions cross sections, nuclear masses, β -decay rates, and other nuclear properties are fundamental inputs to understand the structure, evolution and composition of a large variety of cosmic objects, including the Solar System. Figure 1 summarizes the link between the different fields.

The roles of nuclear physics and of astrophysics are well defined. Nuclear physics is dedicated to measure (nuclear experiments) or to calculate (nuclear theory) the fundamental quantities playing a role in the stellar processes, to extrapolate the cross section data down to astrophysical energies, and to interpret the results using theoretical models. It also has the role of calculating the reaction rates that will allow the astrophysicists to model the different stellar environments and to study the evolution of the stars. Reciprocally, by modelling the impact of the nuclear uncertainties one obtains important indications on the key reactions and the key quantities that have to be studied in the laboratory. Finally, by the astronomy, the experimental data face the observations (γ -radioactivity of the galaxy, element abundances obtained by spectroscopy, supernova light-curves, ...) as well as the results of the analysis of meteorites and grains. The interaction nuclear physics–astrophysics–astronomy must be considered to yield an entire comprehension of the Universe (see Fig. 1).

Whatever the process considered is (primordial, stellar or explosive nucleosynthesis), the calculation of element abundances and the codes of stellar evolution request a huge number of nuclear reaction cross sections. The stellar environment being considered determines the energy region within which the nuclear reaction processes need to be determined. This region is known as the Gamow window [6, 13], and the specific nuclear properties within this energy domain can play a vital role in determining the nucleosynthesis that occurs. Thus, a reaction that may play an important role in a certain stellar environment can be completely negligible under different temperature and density

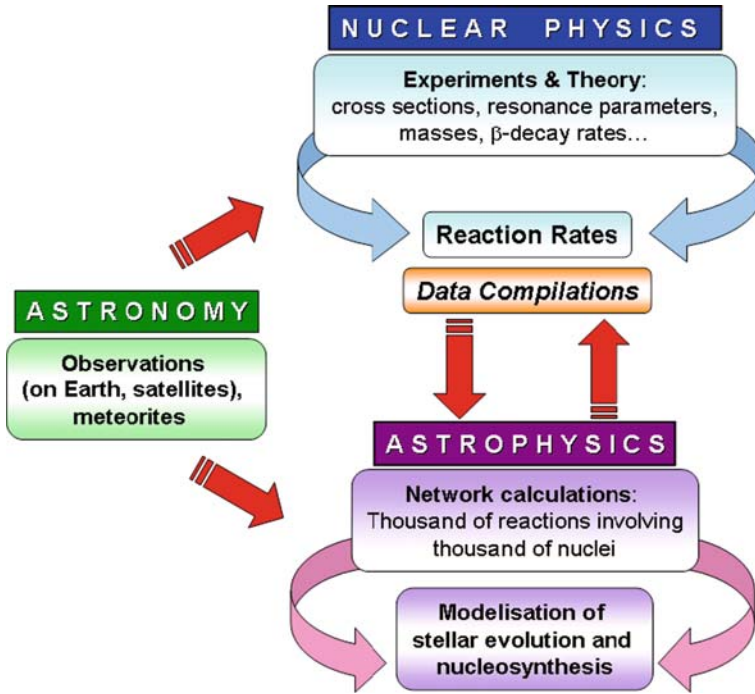


Fig. 1. Link between nuclear physics, astrophysics and astronomy and their respective tasks within nuclear astrophysics [12] (See also Plate 28 in the Color Plate Section)

conditions. Therefore, each nuclear reaction must be treated as a unique process [14]. Most of these reactions involve charged particles whose relative energy, that depends on the temperature of the star, is in general much smaller than the Coulomb barrier of the nuclear systems. Because the probability to tunnel the barrier decreases rapidly with energy, the cross sections of astrophysical interest are among the smallest ever studied in the laboratory (of the order of 10^{-9} b and less) and remain largely uncertain in many cases [15].

Among the many astrophysical sites where nuclear reactions occur, explosive environments such as novae, supernovae and X-ray bursts are particularly fascinating cases. They represent dramatic events that are characterized by high temperatures and densities and produce energy at a rate greater than in almost any other astrophysical phenomena. Under such conditions the interaction times are short enough to be of the order of the lifetimes of the β -radioactive nuclei that will be largely involved in the reaction networks [14, 16]. The sequence of reactions involving such loosely bound nuclei is determined by a balance between proton and α capture rates and rates for β decay or photo dissociation. Hundreds of different reactions involving radioactive nuclei may lie along the reaction path, and unfortunately

our current knowledge concerning the properties of these nuclei and reaction rates is typically very incomplete. The information needed includes nuclear masses, excited state properties, decay properties and lifetimes, electron capture rates, neutrino and photon interaction rates, as well as light particle reaction rates [16]. To gain such information for unstable nuclei is experimentally very challenging as, for instance, typically weak intensities of radioactive ion beams require the use of efficient and highly selective experimental techniques. Knowledge of individual reaction rates is of critical importance. In many situations, there is no alternative other than to measure the properties of individual resonances.

Indeed, the production and acceleration of radioactive beams have completely changed nuclear astrophysics studies in recent years (see, for example, [17] for a review on the techniques of production of radioactive beams). However, in spite of numerous efforts there are still very few laboratories capable of delivering radioactive beams with characteristics (energy range, intensity, stability, isobaric purity) that make them useful for studies of nuclear reactions of astrophysical interest. For some nuclei, especially those at the high- Z end of the r -process path, this information will remain inaccessible for many years to come. In all cases, a rigorous theoretical treatment is necessary to extrapolate the cross sections from the experimentally measured values to the energies characterizing the astrophysical processes [18] and to calculate quantities not accessible in the laboratory.

In the following, the main quantities used in nuclear astrophysics (cross section, S -factor, resonance strength, Gamow window) are introduced. The principal burning cycles are schematically presented and some key reactions are discussed. Some promising experimental techniques are presented and some recent important results are highlighted. Complementary information may be found in recent reviews (see, for example [16, 19, 20]).

2 Relevant Quantities at Stellar Energies

Fusion reactions in stellar plasma involve charged particles and neutrons.² In addition to the nuclear force, the interaction implies the electrostatic repulsive force between the nuclei described by the Coulomb barrier E_C . For energies well-below the Coulomb barrier, which is always the case in the energy range relevant for astrophysics, the probability for penetrating the barrier, \mathcal{P}_ℓ , can be approximated by the so-called Gamow factor for $\ell = 0$ (usually dominating at low energies) [6]:

$$\mathcal{P}_0 \approx \exp(-2\pi\eta(E)), \quad (1)$$

where E is the energy in the centre-of-mass reaction system and $\eta(E)$ is the Sommerfeld parameter,

² Only charged-particle induced reactions are discussed here, see, for example, the review article [4] for neutron-induced reactions.

$$\eta(E) = \frac{Z_1 Z_2 e^2}{\hbar v}, \quad (2)$$

with Z_1, Z_2 being the charge number of the interacting nuclei, e the electron charge, $\hbar = h/2\pi$ (h is the Planck constant), and v the relative velocity of the nuclei. Numerically, $\eta(E) = 0.1575 Z_1 Z_2 (\mu/E)^{1/2}$, with $\mu = M_1 M_2 / (M_1 + M_2)$ being the reduced mass of the system, M_1 and M_2 the masses of the nuclei, and E the energy in MeV. On the other hand, the cross section $\sigma(E)$ is proportional to a geometrical factor $\pi/k^2 \propto 1/E$ (k is the wavenumber). These two factors, \mathcal{P}_0 and π/k^2 , explicitly represent the non-nuclear dependence of $\sigma(E)$. One can thus write the cross section, for energies $E \ll E_C$, as the product of three factors [21]:

$$\sigma(E) = S(E) \frac{1}{E} \exp(-2\pi\eta(E)). \quad (3)$$

This equation defines the so-called astrophysical S -factor, $S(E)$, that contains all the information related to the nuclear properties of the interacting nuclei (resonances, subthreshold states, resonance interferences, ...). If the $\ell = 0$ partial wave is dominant, the S -factor for non-resonant reactions is nearly independent of the energy. If the contribution of other partial waves ($\ell > 0$) are important, the energy dependence of the S -factor cannot be neglected at astrophysical energies. This is the case, for example, of the reactions $d(p,\gamma)^3\text{He}$ reaction, $d(d,\gamma)^4\text{He}$ and $d(\alpha,\gamma)^6\text{Li}$ [15]. Bound states near the reaction threshold (negative energy) can strongly influence the low-energy cross section. The most famous case is the $^{12}\text{C}(\alpha,\gamma)^{16}\text{O}$ reaction that determines the ratio $^{12}\text{C}/^{16}\text{O}$ after helium burning and, thus, the evolution of massive stars [6]. Two subthreshold states dominate its cross section at the astrophysical energies ($E \simeq 300$ keV). In addition, interference with states above threshold strongly complicate the determination of its reaction rate that should be known to better than 20% in order to allow one to draw significant conclusions. But, because its cross section is of the order of 10^{-27} b, it cannot be experimentally determined at the astrophysically relevant energies (the cross section values presently accessible in the laboratory are of the order of 10^{-12} b [22]).

The quantity used in nucleosynthesis calculations is the thermonuclear reaction rate, which is a function of the density of the interacting nuclei, their relative velocity and the reaction cross section. Most of its lifetime, a star is in hydrostatic equilibrium: the gravitational pressure is compensated by the thermal pressure due to nuclear burning, the gas is non-degenerated and the particles are non-relativistic. Under these conditions the velocity distribution is given by the Maxwell–Boltzmann distribution. By using Eq. (2), the reaction rate for a pair of projectile and target nuclei is given by [6]:

$$\langle \sigma v \rangle = \left(\frac{8}{\pi \mu} \right)^{1/2} \frac{1}{k_B T} \int_0^\infty S(E) \exp\left(-\frac{E}{k_B T} - 2\pi\eta(E) \right), \quad (4)$$

where T is the temperature of the stellar interior and k_B the Boltzmann constant. This definition implies the evaluation of an integral from zero to infinity.

Table 1. Values of $E_0 \pm \Delta E_0/2$ and E_C/E_0 for some reactions of the proton–proton chains at $T_9 = 0.015$ (see text)

Reaction	$E_0 \pm \Delta E_0/2$ (keV)	E_C/E_0
p(p, $\nu e+$)d	5.9 ± 3.2	46
d(p, γ) ^3He reaction	6.5 ± 3.4	40
$^3\text{He}(^3\text{He},2\text{p})^4\text{He}$	21.4 ± 6.0	43
$^3\text{He}(\alpha,\gamma)^7\text{Be}$	22.4 ± 6.2	39
$^7\text{Li}(\text{p},\alpha)^4\text{He}$ reaction	14.8 ± 5.0	46
$^7\text{Be}(\text{p},\gamma)^8\text{B}$	17.9 ± 5.5	50

However, because the factor $\exp(-E/k_{\text{B}}T)$ decreases rapidly with energy and the factor $\exp(-2\pi\eta(E))$ increases rapidly with energy, the integrand needs to be evaluated only in a relative narrow energy range called the Gamow window [6, 13] centred around an energy $E_0 = 0.122\mu^{1/3}(Z_1Z_2T_9)^{2/3}$ MeV (T_9 is the temperature in units of 10^9 K). By approximating this energy region by a Gaussian function, one gets a FWHM value given by $\Delta E_0 = 0.2368(Z_1^2Z_2^2\mu)^{1/6}T_9^{5/6}$ MeV. In Table 1, the values of the Gamow window, $E_0 \pm \Delta E_0/2$, as well as the ratio E_C/E_0 are given for some relevant reactions of the proton–proton chains at a typical temperature $T_9 = 0.015$ (centre of the Sun). E_C is calculated as in [23].

Because the cross section does not show details, the advantage of introducing the S -factor is obvious. Figure 2 shows the cross section and the S -factor of the $^3\text{He}(^3\text{He},2\text{p})^4\text{He}$ reaction, which is a typical non-resonant reaction. It has been the first reaction to be investigated in the laboratory at energies within the Gamow window [22, 24, 25].

For a resonant reaction, the cross section can be approximated by a Breit–Wigner expression. Thus the reaction rate depends exponentially on the resonant energy E_{R} and on the resonance strength, $\omega\gamma$ [6]:

$$\langle\sigma v\rangle \cong \left(\frac{2\pi}{\mu k_{\text{B}}T}\right)^{3/2} \hbar^2(\omega\gamma) \exp\left(-\frac{E_{\text{R}}}{k_{\text{B}}T}\right), \quad (5)$$

where $\omega\gamma$ is defined by:

$$\omega\gamma = (1 + \delta_{12}) \frac{2J + 1}{(2I_1 + 1)(2I_2 + 1)} \frac{\Gamma_i \Gamma_f}{\Gamma_{\text{tot}}}, \quad (6)$$

with J being the resonance spin, I_1 and I_2 , the spin of the nuclei, Γ_i (Γ_f) the initial (final) width, and $\Gamma_{\text{tot}} = \Gamma_i + \Gamma_f + \dots$ the total width of the state that should contain all open channels. The spin J is the result of the coupling $\vec{J} = \vec{I}_1 + \vec{I}_2 + \vec{\ell}$. Equation (6) is valid only if the resonance is narrow ($\Gamma_{\text{tot}} \ll \Delta E_0$). For broad resonances the calculation of the reaction rate must be performed numerically [18]. At low energies, the resonant rate essentially

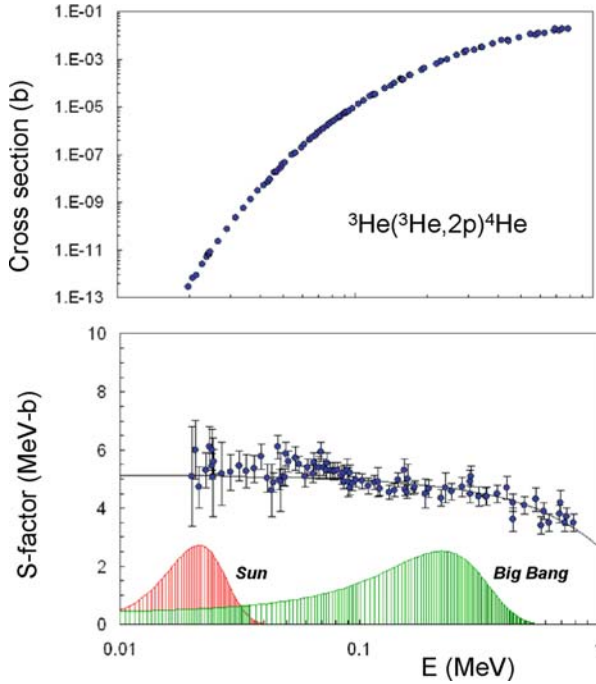


Fig. 2. Cross section and S -factor of ${}^3\text{He}({}^3\text{He},2p){}^4\text{He}$ (data are taken from [15]). The *solid curve* is a theoretical extrapolation. The Gamow window for $T_9 = 0.015$ (Sun) and $T_9 = 0.5$ (Big Bang) are indicated (See also Plate 29 in the Color Plate Section)

depends on the resonances with lower kinetic moments, generally $\ell = 0$. For example, the reaction rate of ${}^{13}\text{N}(p,\gamma){}^{14}\text{O}$, which is the first reaction of the hot CNO cycle, is dominated (at $T_9 < 1$) by a $J^\pi = 1^-$ ($\ell = 0$) resonance at $E_R = 528.4$ keV [15]. On the contrary, the $J^\pi = 1^+$ ($\ell = 1$) resonance of the ${}^7\text{Be}(p,\gamma){}^8\text{B}$ reaction is negligible at energies $E < 300$ keV [26].

Resonances with different ℓ values do not interfere among each other as far as the integrated cross section is concerned [18]. In general, if the angular momentum of the resonance ℓ_R is different from the lower value ($\ell = 0$), the contribution of the resonance is added to the non-resonant contribution, the latter being essentially that obtained for $\ell = 0$, $\sigma(E) \approx \sigma_{\ell_R}(E) + \sigma_{0,\text{NR}}(E)$. This is the case for ${}^7\text{Be}(p,\gamma){}^8\text{B}$, where the S -factor is dominated by the asymptotic behaviour of the Coulomb functions at $E = 0$. On the contrary, if the resonance angular momentum ℓ_R is zero, the total cross section depends on that resonance and thus, $\sigma(E) \approx \sigma_{\ell_R}(E)$, with the contribution of the other angular momenta $\ell \neq 0$ being strongly attenuated. Reactions such as ${}^{12}\text{C}(p,\gamma){}^{13}\text{N}$ and ${}^{13}\text{N}(p,\gamma){}^{14}\text{O}$ are examples of such a behaviour.

3 Stellar Cycles and Some Key Reactions

The first burning stage of a star is hydrogen burning that occurs typically at a temperature of the order of 10^7 K. From all the nuclear reactions involved in the proton–proton chain, ${}^3\text{He}(\alpha,\gamma){}^7\text{Be}$ is especially interesting as it is the main source of uncertainty in determining the solar neutrino flux at higher energies [27] which results from the β decay ${}^8\text{B}(e^+\nu){}^8\text{Be}$ following the reaction ${}^7\text{Be}(p,\gamma){}^8\text{B}$. It also plays a role determining the primordial ${}^7\text{Li}$ abundance, although the ${}^3\text{He}(\alpha,\gamma){}^7\text{Be}$ uncertainties do not explain the ${}^7\text{Li}$ problem [28]. Data on the ${}^3\text{He}(\alpha,\gamma){}^7\text{Be}$ cross section were obtained so far by using two different methods, i.e. direct γ -ray detection and detection of ${}^7\text{Be}$ radioactivity [15]. The results of recent experiments [29, 30] are in agreement with an earlier data compilation [31]. New studies are underway at the LUNA Gran Sasso Laboratory.

The CNO cycle is the main energy source for stars that are somewhat more massive than the Sun (at $T \simeq 2\text{--}5.5 \times 10^7$ K). However, all stars produce energy via the CNO cycle at the end of their main sequence lifetimes, and while on the red-giant branch. At present, the reactions that play the more important role in the CNO cycle are: ${}^{14}\text{N}(p,\gamma){}^{15}\text{O}$, ${}^{17}\text{O}(p,\gamma){}^{18}\text{F}$, and ${}^{17}\text{O}(p,\alpha){}^{14}\text{N}$. The latter two reactions on ${}^{17}\text{O}$ are also of interest in explosive burning, as will be shown below. The ${}^{14}\text{N}(p,\gamma){}^{15}\text{O}$ reaction is the slowest one in the CNO cycle and thus regulates the rate of nuclear energy generation. The power liberated by the CNO cycle and the amount of helium produced are related to the luminosity observed at the transition between the main-sequence and the red-giant branch, and to the luminosity of the horizontal branch. Both of these quantities play a role in determining the ages of globular clusters [32–34].³ Moreover, since it helps to constrain the temperature and density profiles in the hydrogen-burning shell, ${}^{14}\text{N}(p,\gamma){}^{15}\text{O}$ will affect nucleosynthesis beyond the CNO cycle during the red-giant stage [35, 36]. Two recent, direct and independent studies [35, 37] are presented in more detail in Sect. 4. Important astrophysical consequences are also discussed there.

Hydrogen burning explains the nucleosynthesis of elements with $A \leq 4$ (the elements with $A = 7$ are not produced in sufficient amount by the p–p chain to survive hydrogen extinction). Therefore the more plausible explanation of the ratio $\text{He}/\text{H} \sim 0.2$ comes from hydrogen burning produced at the primordial Universe about 13 billions of years ago. Hydrogen burning is followed by a gravitational contraction until the centre of the star reaches a temperature sufficiently high for the ignition of helium burning (typically at about 2×10^8 K) [6, 13]. After hydrogen and helium, the more abundant elements are carbon and oxygen. Because ${}^8\text{Be}$ is not stable, the fusion process $\alpha + \alpha$ only represent an intermediate state in the ${}^{12}\text{C}$ synthesis. Because ${}^{12}\text{C}$ and ${}^{16}\text{O}$

³ The globular clusters are old stellar objects presenting heavy-element abundances much lower than those of the main sequence stars. They have presumably been formed from primordial matter, before galaxy formation. They are thus an unique “stellar laboratory” to determine the age of the Universe.

are composed of a number of protons and neutrons equivalent to three and four α particles, respectively, they can be synthesized by three-body reactions, i.e. $3\alpha \rightarrow {}^{12}\text{C} + \gamma$. Only because the $\alpha + {}^8\text{Be}$ reaction is resonant (the Hoyle state at an energy of 278 keV above threshold [38]), ${}^{12}\text{C}$ is produced in sufficient amount to account for the stellar abundances. Another state at about 10 MeV in ${}^{12}\text{C}$ has been also observed [39] but its influence in the triple- α process remains to be firmly established [40]. The triple- α reaction dominates helium burning in the more evolved burning phases [36].

After the triple- α process, helium burning continues through the chain of reactions ${}^{12}\text{C}(\alpha, \gamma){}^{16}\text{O}(\alpha, \gamma){}^{20}\text{Ne}$. The last one is negligible except for very massive stars (more than 30 times the solar mass) [6]. ${}^{12}\text{C}(\alpha, \gamma){}^{16}\text{O}$ is one of the more important reactions in astrophysics, its cross section at 0.3 MeV (position of the Gamow window for a typical temperature of 0.25 GK) is of the order of 10^{-27} b, comparable to that of the weak interaction. Contrary to the triple- α process, ${}^{12}\text{C}(\alpha, \gamma){}^{16}\text{O}$ is practically a non-resonant reaction at that energy and its cross section is given by the tails of interfering resonance and subthreshold states. A lot of experimental efforts has been dedicated to the study of this reaction. For a detailed review, see, for example, the recent paper of Buchmann and Barnes [41].

In parallel to the main chain, ${}^{14}\text{N}$, the main ash of the CNO cycle, is transformed into ${}^{22}\text{Ne}$ by a chain of two α -capture reactions and one β decay, namely ${}^{14}\text{N}(\alpha, \gamma){}^{18}\text{F}(\beta^+){}^{18}\text{O}(\alpha, \gamma){}^{22}\text{Ne}$. ${}^{22}\text{Ne}$ is one of the main neutron sources due to the ${}^{22}\text{Ne}(\alpha, n){}^{25}\text{Mg}$ reaction and thus an important path to the s -process. The ${}^{22}\text{Ne}(\alpha, n){}^{25}\text{Mg}$ reaction cross section remains largely uncertain [15]. The other important neutron source in massive stars is ${}^{13}\text{C}(\alpha, n){}^{16}\text{O}$ [42]. Its cross section, measured at energies above 0.3 MeV [43, 44], strongly depends on a $1/2^+$ state situated at 3 keV below threshold [45]. The extrapolation to astrophysical energies remains very uncertain.

A sequence of further reactions gradually transform the hearth of stars into heavier and heavier nuclei. The energy produced balances the gravitational contraction. However, once the thermal pressure is not sufficient to balance the gravitational force the hearth contracts and the temperature increases enough to ignite the ashes of previous burning phases. Thus, the helium burning ashes in massive stars are the fuel of successive nuclear processes. After helium burning, and depending on the mass of the star, phases burning carbon, oxygen, neon and silicon will successively take place to produce iron. The last possible step is explosive burning [13].

Explosive burning takes place at much higher temperatures and densities during events such as novae, supernovae and X-ray bursts. Nucleosynthesis in novae (temperatures $T \simeq 2-3 \times 10^8$ K, densities $\rho \simeq 10^3$ g/cm³) involves about 100 stable and radioactive nuclei ($A < 40$) and a few hundred reactions [46], mainly (p, γ) and (p, α) reactions with the nucleosynthesis path located at the border of nuclear stability. Data needed for nova models are essentially rates of reactions involving stable and radioactive nuclei and β -decay half lives. The situation is more complex for X-ray bursts

($T \simeq 10^9$ K, $\rho \simeq 10^6$ g/cm³) as the main sequence of reactions is far from stability, reaching the proton drip line above $A = 38$ [47]. The data needed when modelling these stellar systems are the cross sections for proton and α -induced reactions on stable and radioactive nuclei and for photodissociation as well as the β -decay half lives, for a few hundred nuclei with masses $A \leq 110$ [48]. This means that several thousand reactions are involved [49]. Recent experiments are dedicated to a series of important reactions in nova nucleosynthesis: $^{17}\text{O}(p,\gamma)^{18}\text{F}$ and $^{17}\text{O}(p,\alpha)^{14}\text{N}$ (direct and indirect studies at TUNL and CSNSM Orsay) [50–52], $^{21}\text{Na}(p,\gamma)^{22}\text{Mg}$ (direct studies at TRIUMF and indirect studies at KVI) [53–55], $^{22}\text{Na}(p,\gamma)^{23}\text{Mg}$ (indirect studies at ANL) [56], $^{23}\text{Na}(p,\gamma)^{24}\text{Mg}$ and $^{23}\text{Na}(p,\alpha)^{20}\text{Ne}$ (direct studies at TUNL) [57], and $^{30}\text{P}(p,\gamma)^{31}\text{S}$ (indirect studies at ANL) [58]. A lot of effort has been dedicated to the $^{18}\text{F}(p,\alpha)^{15}\text{O}$ reaction, which is the main destruction reaction of ^{18}F ($T_{1/2} = 110$ min) during nova outbursts and thus related to detection of γ -rays from novae by future satellite missions. Its cross section needs to be known at energies as low as 200 keV (see, for example, [59]). This reaction will be discussed in detail in Sect. 4.5.

Figure 3 shows schematically the relation between stellar sites and nuclear processes. A detailed discussion can be found in Chap. 5 of [6].

4 Experimental Techniques in Nuclear Astrophysics

The experimental techniques used to investigate nuclear quantities of astrophysical interest are very varied and depend on the stellar environment under investigation (quiescent or explosive burning). Some relevant issues are discussed in the following.⁴ To illustrate the experimental techniques typically used in nuclear astrophysics studies, three selected examples of reaction studies are described in more detail.

4.1 Targets

The measurement of reaction cross sections at very low energies with intense stable-isotope beams (of the order of mA) and water-cooled thick solid targets requests the monitoring of the stability and of the stoichiometry of the target as a function of the beam dose. This is typically performed by measuring from time to time the cross section at a reference energy (target stability) and by nuclear reaction analysis before and after the target has been employed (target stoichiometry). The appropriate corrections must be applied to the experimental results [13].

The study of reactions involved in explosive astrophysical process requires the development of radioactive beams [17]. Reactions involving hydrogen and helium are the most important ones in explosive burning. Because

⁴ The choice here is exclusively based on the author's preferences and experience.

<u>Stellar site</u>	<u>Nuclear process</u>
Big Bang (primordial nucleosynthesis)	<u>Reactions between light elements</u> p, d, He, Be, Li <u>Hydrogen burning</u> Proton-proton chains, CNO cycle, Ne-Na cycle, Mg-Al chain
Main sequence stars (ex. the Sun)	
Red giant stars Asymptotic giant branch (AGB) stars	<u>Helium burning</u> 3 α process, $^{12}\text{C}(\alpha,\gamma)^{16}\text{O}$, Other (α,γ) and (α,n) reactions
Super giant stars Wolf-Rayet stars Pre-supernovae	
Novae Supernovae X-ray bursts	<u>Advance burning stages</u> Reactions of C, O, N, Ne, Si... <u>Explosive burning</u> Hot CNO cycle Rapid proton capture (rp-process)
AGB stars Supernovae type-II Neutron stars	
	<u>Nucleosynthesis beyond iron</u> Slow neutron capture (s-process) Rapid neutron capture (r-process) Photodisintegration and proton capture (p-process)

Fig. 3. Relation between astrophysical sites and nuclear processes [12]

the lifetime of the interacting nuclei are too short to allow one to produce targets, inverse kinematics methods using radioactive beams require the use of hydrogen-rich or helium-rich targets. The choice of the target must be adapted to the physics goal and the other experimental conditions (such as beam energy and intensity, detection system, etc). Polyethylene foils $[(\text{CH}_2)_n]$ are easy to handle and have been one of the most popular and successful targets for investigation of hydrogen burning reactions. Foils with thicknesses between $40\ \mu\text{g}/\text{cm}^2$ and several mg/cm^2 have been used with beam intensities as high as $10^9\ \text{s}^{-1}$ [60, 61] without significant degradation, though care must be taken to distribute the beam power by, for example, rotating the target. Solid targets containing helium are produced by implantation. Implanted helium targets have been developed at Louvain-la-Neuve with helium thicknesses up to $10^{18}\ \text{atoms}/\text{cm}^2$, sufficient for measurement of elastic scattering and some reactions with radioactive ion beams [62]. Gas targets are an obvious alternative to foils. Gas cells with thin windows are easy to handle, but the windows produce similar challenges as with foil targets, degrading the beam energy and inducing background reactions. Windowless gas targets eliminate the problems associated with windows. However, many

pumping stations are required to decrease the pressure to the 10^{-7} mbar range required when performing on-line experiments at accelerators. Hence the gas targets are large and costly, and the target thickness is limited [63].

4.2 Detectors

Studies of capture reactions of interest in quiescent burning are mainly limited by the cosmic background of the γ detectors. One can build a lead wall around the detectors but the interaction of the cosmic rays with the material will produce γ -rays and neutrons that will also affect the measurements. Another possibility to partially reduce the activation problem is an active shielding using, for example, plastic scintillators operated in anti-coincidence with the γ detectors. The best (but not always the easiest) solution is going underground [64]. The pioneers of underground laboratories for nuclear astrophysics reaction measurements is the LUNA laboratory, situated under the Gran Sasso mountain in Italy. Its unique character is a suppression of the cosmic rays equivalent to 4,000 m of water. Two linear accelerators that are installed at LUNA (50 and 400 keV) have allowed to measure cross sections of the order of 0.01 pb [22]. An example of these measurements at the limits of the technical possibilities is the study of the $^{14}\text{N}(p,\gamma)^{15}\text{O}$ reaction [37]. In the United States, a new project for the construction of an underground laboratory has been recently launched by a collaboration of several universities and laboratories from US and Europe.

In studies involving radioactive beams, the low-beam intensities (at present, typically of the order of 10^4 – 10^8 s^{-1} on target) require the use of very efficient detection systems. Arrays of γ , neutron and charged-particle detectors have been constructed at many facilities in order to maximize the detection efficiency [16]. The advent of large-area silicon strip detectors covering a large solid angle has played a crucial role. These detectors may be segmented in one or two dimensions (doubled-sided detectors) to any practical level of pixelation. The shape of the strips can also be tailored to experimental requirements. For example, strips are curved in a circular pattern in many annular detector designs to allow better reaction angle resolution in a strip. This approach was used in the Louvain–Edinburgh detector array (LEDA), one of the pioneering charged-particle arrays used with radioactive ion beams for nuclear astrophysics [65]. LEDA is composed of independent 16-strip sectors. Its typical electronic resolution is of the order of 10 keV, the energy resolution for 5.5 MeV α particles is about 20 keV, while the time resolution is of about 1 ns. Figure 4 shows a schematic drawing of one of the LEDA sectors and a typical experimental setup using two LEDA arrays. A broader range of detector thicknesses has recently become available, and detectors between 50 μm and 1 mm are common. This broad range of thicknesses allows Z identification of a broad range of charged particles through $\Delta E - E$ techniques. These detectors require new associated electronic modules and new data acquisition systems capable to work with a large number of signal chan-

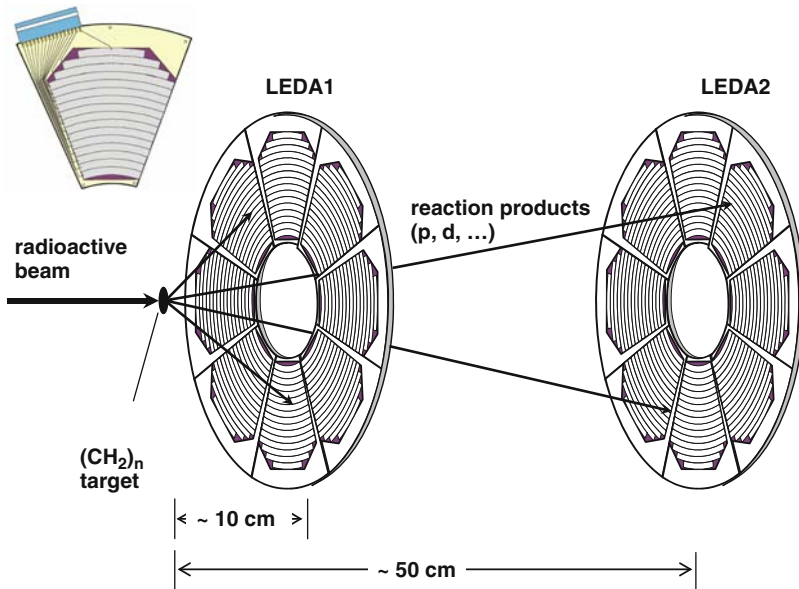


Fig. 4. Typical experimental setup for the measurement of a transfer reaction by means of the LEDA detector [65]. The insert on the *top left* is a schematic drawing of one LEDA sector (See also Plate 30 in the Color Plate Section)

nels and a small deadtime. Also because of the very low-beam intensities it is not possible to use the conventional methods to measure the accumulated beam dose with sufficient precision. In the measurement of cross sections or of resonance strengths, the absolute normalization is always one of the most important tasks. One of the techniques successfully employed is to evaporate a very thin gold layer on the target (when using a plastic foil as a target) and normalize to the measurement of the Rutherford cross section [66].

Arrays of γ -ray detectors have played an important role in several new approaches using both stable-isotope and radioactive ion beams. For instance, the high-total efficiency of the Gammasphere array [67] allowed $\gamma - \gamma$ coincidence measurements. They accurately determined excitation energies of levels in proton-rich nuclei that are of astrophysical importance. Some of the problems with direct measurements, mainly the low efficiency of γ -detectors, the radioactivity of the target material, and the background sources can be solved by performing measurements in inverse kinematics and detecting the recoiling reaction products in recoil separators. This technique is briefly described in Sect. 4.3.

4.3 Recoil Separators

Recoil separators are devices which separate the nuclear reaction products (recoils) leaving the target from the primary beam and focus the former onto a

detector system [68]. The experimental challenge is to maintain a high transmission of the heavy reaction recoils while maximizing the rejection of the primary beam. This is difficult because of the small mass and momentum difference between the projectiles and recoils. It is also difficult because all the projectiles enter the separator, their intensity being typically $10^{10} - 10^{15}$ times larger than of the recoils. To obtain the maximum separation, the primary beam is blocked at an early stage of the separator. Some recoil separators have the additional property of dispersing the reaction products at the focal plane according to their mass-to-charge ratio. The scattered beam rejection is enhanced by filtering out particles on the basis of both velocity and ratio between both mass and ionic charge, which necessitates the use of either velocity filters combined with magnetic dipoles or a combination of electric and magnetic dipole elements.

A recoil separator suitable for (p,γ) and (α,γ) studies in astrophysics should have the following specifications [68]:

- (i) High-transport efficiency for a relative small solid angle (typically less than 5 msr): due to the inverse kinematics, the maximum angles of the ejectiles should peak near 0° .
- (ii) High-beam rejection over a broad mass range of beams.
- (iii) Relative low-mass resolution ($\delta M/M \leq 0.5\%$).
- (iv) Target chamber capable of accommodating a variety of detector arrays and gas targets (both jet and extended targets).
- (v) Capability of running with different ion optical modes for reactions with different kinematics.
- (vi) Incorporation of careful beam handling upstream of the separator (e.g. clean recoil beam with small dispersion and no beam halo).

Several laboratories have developed recoil separators that are designed to collect heavy reaction products and disperse them by their mass-to-ionic-charge ratio. Such separators for astrophysical studies are, for example, DRAGON at ISAC (TRIUMF) [63], ERNA at Bochum [69], the Daresbury Recoil Separator at the HRIBF (Oak Ridge) [70], and the FMA at ANL (Argonne) [61]. A new separator dedicated to nuclear astrophysics studies using stable-isotope beams is under construction at the University of Notre-Dame [71].

4.4 Ground State Properties

The β -decay half lives and masses of nuclei are important for understanding explosive processes. Half lives for β decay can be long compared to the time scale for nuclear reactions, and thus the decays of nuclei near the proton drip line can govern energy generation and nucleosynthesis in the explosion. As the rates of nuclear reactions depend exponentially on the reaction Q value, mass measurements are a crucial first step towards determining these rates. The development of highly selective spectrometers, traps, detectors, and

other instrumentation at laboratories around the world has allowed nearly all isotopes of interest for explosive hydrogen burning to be produced and identified in recent years. Half lives and masses, which can be measured with relatively few atoms, are often the first quantities determined experimentally.

Thanks to this impressive world-wide efforts [72–74], now there remain only a few particle-stable neutron-deficient isotopes with $Z < 53$ whose half lives have not been measured with reasonable accuracy. Most important for the rp -process are the last unobserved even–even nuclei below ^{100}Sn , i.e. ^{74}Sr , ^{78}Zr ($N = Z - 2$) and ^{96}Cd ($N = Z$) which could have reasonably long half lives. Although the general progress in studying half lives in this region of the chart of nuclei is indeed impressive, there still exist many isotopes heavier than nickel that lack accurate mass measurements or other experimental information. The techniques developed for capturing and cooling nuclei in traps and storage rings should allow the situation with nuclear masses to be much improved in the near future. However, the additional structure information necessary to extract reaction rates will require substantially more effort.

4.5 Resonances Properties

Some reaction rates at the temperatures of explosive burning are totally or partially dominated by the contribution of resonances. It is therefore important to study the properties of the resonant states using, e.g. elastic and/or inelastic scattering, transfer reactions populating the mirror states, and fusion evaporation reactions. These techniques are discussed in the following subsections.

Elastic and Inelastic Scattering

Applied since the early 1950s [75], elastic scattering is a well-known method to study resonant states. As a natural extension [76, 77], the elastic scattering technique in *inverse kinematics*, used normally to investigate reactions involving radioactive species, makes use of the sensitivity of the protons (or α particles) to the presence of a resonant state in the compound nucleus. Figure 5 shows the principle of the method. The method is based on the fact that the energy loss of heavy ions in a target is significantly larger than the energy loss of protons (which is normally negligible for typical target thicknesses of less than 1–2 mg/cm²). The resulting recoil proton spectrum can be compared to a “snapshot” of a certain energy range in the level scheme of the compound nucleus. The method can also be applied to α scattering, although being less sensitive. Another advantage is that the laboratory energy of the recoil particles (protons or α particles) are rather high and given by:

$$E_{\text{lab}} = E_{\text{cm}} \frac{4A_{\text{p}}}{A_{\text{p}} + A_{\text{t}}} \cos^2 \phi_{\text{lab}}, \quad (7)$$

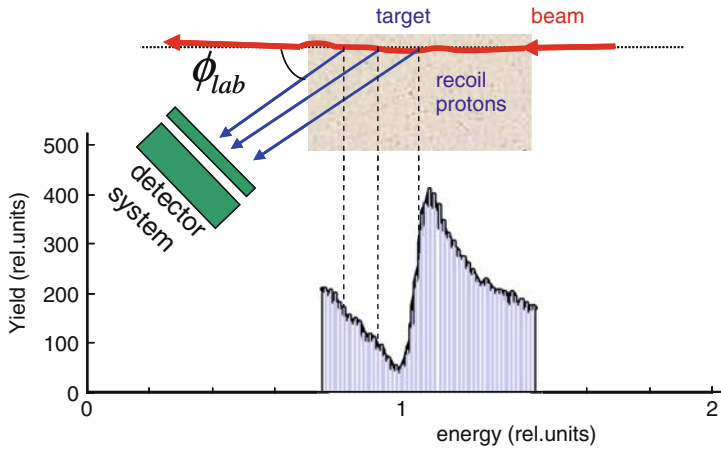


Fig. 5. Principles of the elastic scattering method in inverse kinematics. The spectrum is a typical interference pattern for a $\ell = 0$ resonance (see text) (See also Plate 31 in the Color Plate Section)

where A_p, A_t are the mass number of the projectile and the target nuclei, respectively, and ϕ_{lab} the recoil angle. On the other hand, the cross section for elastic scattering is proportional to the square of two contributions, the Coulomb amplitude and the nuclear amplitude [78]:

$$\left(\frac{d\sigma}{d\Omega} \right)_{\text{elas}} = |f_N + f_C|^2 \quad (8)$$

The nuclear amplitude depends on the collision matrix $U_{\ell I}^{J\pi}$ that can be written as a function of the phase shift [78]:

$$U_{\ell I}^{J\pi} = \exp(2i\delta_{\ell I}^{J\pi}), \quad (9)$$

where J and π are the spin and parity of the resonant state, respectively, I the channel spin and ℓ the angular momentum. When a resonant state is “scanned” with the appropriate combination projectile–target, the recoil proton spectra show an interference pattern that is indicative of the resonance energy, angular momentum and width (see Fig. 5). All experimental effects, mainly the beam energy resolution inside the target and the angular resolution of the detectors, must be properly taken into account to precisely extract the resonant properties. Fitting procedures, such as the R -matrix method [78], are typically used to evaluate these quantities and to obtain the resonance properties.

Elastic scattering measurements with radioactive beams have been widely applied to determine resonant properties that are important for nuclear astrophysics and nuclear structure [66, 79–81]. One of the main advantages is the large cross section for elastic scattering that allows measurements with

radioactive beam intensities as low as 10^4 s^{-1} . Another advantage is that the energy of the recoil protons is usually sufficiently high to be detected readily in standard silicon detectors or in more sophisticated strip detector arrays [65]. The β radioactivity of the beam species may induce background in the particle detectors at low energies. This background can limit the lowest energies measurable, but this time-uncorrelated background can be distinguished from the events of interest by time-of-flight techniques.

A recent example of an elastic scattering measurement of astrophysical interest is the study $^{21}\text{Na}+p$ at the ISAC facility at TRIUMF [82]. An intense ($5 \times 10^7 \text{ s}^{-1}$) ^{21}Na beam at laboratory energies below 1.5 MeV/nucleon bombarded 50–250 $\mu\text{g}/\text{cm}^2$ thick $(\text{CH}_2)_n$ targets. The recoil protons were detected using the TUDA strip detector array [65]. Three strong resonances corresponding to states in ^{22}Mg have been identified at energies of 830, 1115 and 1311 keV, respectively. These states dominate high-temperature burning of ^{21}Na via $^{21}\text{Na}(p,\gamma)^{22}\text{Mg}$ and probably influence the low-temperature stellar rate of this reaction. However, to determine the γ strengths and other properties of these states, additional radiative capture measurements are needed [83].

In an inelastic scattering process, the energy of the collision is sufficiently high to excite one of the interacting nuclei. This method becomes particularly important when one attempts to extract a reaction rate from cross section measurements of the inverse reaction. For example, the $^{17}\text{F}(p,\alpha)^{14}\text{O}$ cross section has been measured at energies that allow the inverse $^{14}\text{O}(\alpha,p_0)^{17}\text{F}_{gs}$ reaction rate to be determined by detailed balance [84, 85]. However, the contribution of the $^{14}\text{O}(\alpha,p_1)^{17}\text{F}^*$ reaction branch to the 495 keV first excited state of ^{17}F is not determined by the inverse reaction measured on nuclei in their ground state. Both elastic and inelastic scattering of $^{17}\text{F}+p$ were measured at Argonne National Laboratory [86] and at the Holifield Radioactive Ion Beam Facility (HRIBF) [87] to study states in ^{18}Ne that are important for the $^{14}\text{O}(\alpha,p)^{17}\text{F}$ reaction.

Another example is the measurement of $^{19}\text{Ne}(p,p_1)^{19}\text{Ne}^*$ recently performed by a GANIL–Louvain–Edinburgh collaboration at the CRC in Louvain-la-Neuve. The goal was to determine the properties of the ^{19}Ne states near the $^{18}\text{F}+p$ threshold (see Sect. 4.5). Data analysis is ongoing.

Transfer Reactions

Much of our understanding of nuclear spectroscopy has been shaped by the study of transfer reactions in the last decades. These have proved to be a particularly powerful tool for characterizing energy levels of importance for astrophysical reactions. One advantage of these measurements is that states covering a broad region of excitation energy are populated. The main disadvantage from the experimental point of view is that this method needs high-resolution particle detection in order to resolve the states of interest. In addition, difficult targets and problematic kinematics make studies of resonant states via proton transfer in inverse kinematics particularly challenging.

On the theoretical side, many of these reactions can be described by the distorted-wave born approximation (DWBA) which predicts that the shape of the angular distribution of the differential cross section is distinctive of the transferred angular momentum, and the magnitude of the cross section reflects the single-particle character of the state [88]. However, the results are usually model-dependent. Proton-transfer reactions, for example ($^3\text{He},d$), are the best surrogate for proton-induced reactions like (p,γ). The (d,p) neutron-transfer reaction has also been used to indirectly obtain information on single-particle resonances. The properties of neutron single-particle states are studied by the (d,p) reaction on the mirror nucleus, and the properties of proton resonances are determined under the assumption of mirror symmetry. This technique was first applied with a radioactive ion beam to ^{56}Ni at Argonne National Laboratory [89] and it has been used more recently to study the $^{18}\text{F}(p,\alpha)^{15}\text{O}$ at Louvain-la-Neuve [90, 91] and at the HRIBF [92, 93] (see Sect. 4.5).

Reactions like (p,t) [94], ($^3\text{He},n$) [95, 96] and ($^3\text{He},^6\text{He}$) [97, 98] have been extensively studied. The distinctive Q -values for these reactions typically allow for a high selectivity for charged particle detection in high-resolution magnetic spectrographs. Comparable resolution is also possible with the ($^3\text{He},n$) reaction using time-of-flight techniques with only a modest flight path. For example, states in ^{26}Si that are important for the $^{25}\text{Al}(p,\gamma)^{26}\text{Si}$ reaction were studied at the Edwards Accelerator Laboratory at Ohio University using the $^{24}\text{Mg}(^3\text{He},n)^{26}\text{Si}$ reaction [99]. Neutrons were detected with a flight path of 10 m, and a resolution of about 16 keV was achieved in the region of interest.

More exotic reactions, such as ($^3\text{He},^8\text{Li}$) [100], ($^4\text{He},^8\text{He}$) [101], ($^7\text{Li},^8\text{He}$) [102, 103] and ($^{12}\text{C},^6\text{He}$) [96], have also been used to study states of nuclei further away from stability by means of stable-isotope beams and targets. The mechanisms of such reactions are complex, and the cross sections are typically small. However, in some cases high-intensity stable-isotope beams can be used to achieve reasonable reaction yields. States of unnatural parity are sometimes populated with comparable yields to natural parity states, allowing states to be studied that are weakly populated in direct reactions. For example, states of unnatural parity in ^{26}Si , that dominate the rate of the $^{25}\text{Al}(p,\gamma)^{26}\text{Si}$ reaction and are thus important for understanding the production of ^{26}Al in novae, were studied using the $^{29}\text{Si}(^3\text{He},^6\text{He})^{26}\text{Si}$ reaction at Wright Nuclear Structure Laboratory (WNSL) at Yale University [104].

Nuclei heavier than nickel in the rp -process are too far away from stable nuclei to be produced by transfer reactions involving stable-isotope beams and targets. Radioactive ion beams are thus required to access these nuclei by transfer reactions. Fragmentation facilities like that at the Michigan State University (MSU) produce nuclei near the rp -process path as beams with sufficient intensity to allow transfer reaction studies. Nucleon knock-out reactions like (p,d) have much more favourable cross sections than stripping reactions at the beam energies available from fragmentation facilities. A set of measurements proposed for MSU will use the (p,d) reaction induced by a radioactive ion beam to populate proton-unbound states of nuclei near the

path of the rp -process. The emitted protons and residual heavy nuclei being detected in coincidence in order to construct excitation energy spectra.

4.6 Selected Examples of Reaction Measurements

The $^{14}\text{N}(p,\gamma)^{15}\text{O}$ Reaction and the Age of the Globular Cluster

The capture reaction $^{14}\text{N}(p,\gamma)^{15}\text{O}$ ($Q = 7.297$ MeV) is the slowest process in the hydrogen burning CNO cycle and thus of high-astrophysical interest. This reaction plays a role in setting the energy production and neutrino spectrum of the sun [27] as well as determining the age of globular clusters cluster [32–34]. Below 2 MeV, several states in ^{15}O contribute to the $^{14}\text{N}(p,\gamma)^{15}\text{O}$ cross section: a $3/2^+$ subthreshold state at -504 keV and three resonant states, $1/2^+$ at 259 keV, $3/2^+$ at 987 keV, and $3/2^+$ at 2187 keV, respectively. Figure 6 shows the level scheme of ^{15}O . Above the $^{14}\text{N}+p$ threshold only the above-mentioned resonant states are indicated.

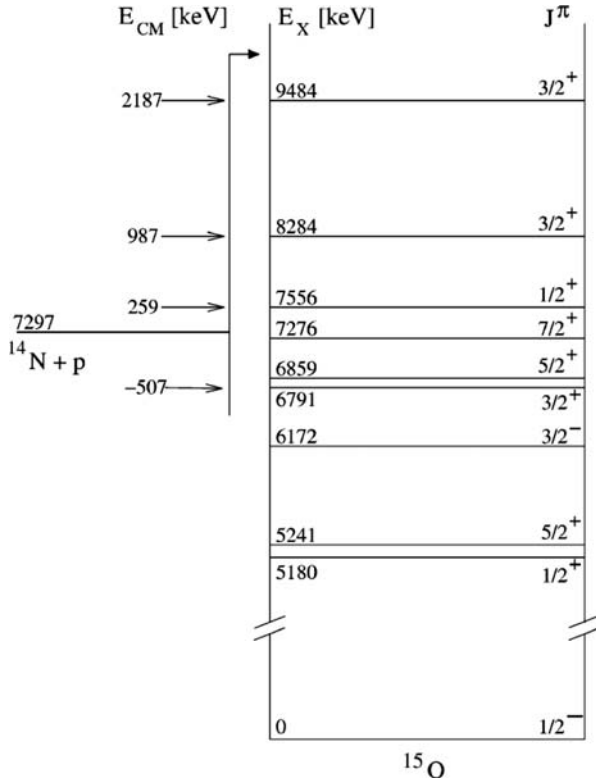


Fig. 6. Level scheme of ^{15}O (from [37]). States relevant for the $^{14}\text{N}(p,\gamma)^{15}\text{O}$ reaction are indicated by *arrows*

A theoretical analysis of previous data [105], using the R -matrix model [106], yielded a difference of a factor of 2 in the rates with respect to those adopted in compilations [15] at the relevant temperatures. This difference is due to the different contribution of the subthreshold state to the capture reaction leading to the ^{15}O ground state, which was found to be negligible in [106]. This result was supported by a lifetime measurement of the subthreshold state via the Doppler-shift [107] and the Coulomb excitation [108] methods. In view of this and of the astrophysical importance of the $^{14}\text{N}(p,\gamma)^{15}\text{O}$ reaction, a new more precise measurement, extending the lower-energy limit below that reached by previous work ($E < 0.24$ MeV), was highly desirable [106].

Two experimental groups have undertaken the study of the $^{14}\text{N}(p,\gamma)^{15}\text{O}$ cross section at low energies, one at the LUNA laboratory at Gran Sasso [37] and the other one at the LENA laboratory at TUNL [35]. The results of the two measurements analysed by using the R -matrix method are in agreement. The result obtained by a simultaneous R -matrix analysis of all existing data sets [109] are shown in Fig. 7. With the present $^{14}\text{N}(p,\gamma)^{15}\text{O}$ rates, the age at the main-sequence turnoff⁵ is 0.5–1.0 Gy older than that deduced from the previous rates. This value depends on the method used to determine the luminosity and the metallicity of the globular clusters even if all other parameters are assumed to be fixed (e.g. distance to globular clusters, time between the

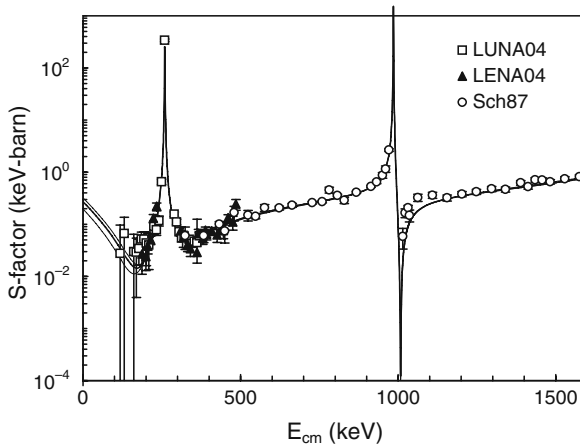


Fig. 7. $^{14}\text{N}(p,\gamma)^{15}\text{O}$ data for the transitions to the ground state in ^{15}O . The experimental results marked by squares, triangle and circles stem from the LUNA [37] and LENA [35] facilities and from the early work of Schöder et al. [105], respectively. The solid curve is the best R -matrix fit [109]. Different curves, corresponding to different R -matrix parameters, are undistinguishable above 0.2 MeV

⁵ The turnoff point is the moment at which the star evolves from the main sequence (central burning phase) to the asymptotic branch of red giants (shell burning phase).

Big Bang and the star formation, etc.) [12]. In addition, the solar neutrino flux from the CNO cycle is reduced by a factor of 2 [27].

For pedagogical purposes, the measurement of the $^{14}\text{N}(p,\gamma)^{15}\text{O}$ cross section at the LENA laboratory [35] (a typical “above-ground” low-energy accelerator) is briefly described in the following. The measurement was performed using a 1 MV Van der Graaff accelerator providing proton beams at laboratory energies between 155 and 524 keV, with beam currents of 100–150 μA . The ^{14}N targets were fabricated by implanting nitrogen ions into a 0.5 mm-thick tantalum backings, that etched in an acid solution to remove surface impurities. The target composition and thickness remained stable over the accumulated doses of 20–25 C. This was regularly checked by measuring the yield curve for the 0.259 MeV resonance (see Fig. 6). A total of 32 independent measurements were performed to obtain the resonance strength of this resonance, yielding good agreement with previous values. Branching ratios for the decay of the 0.259 MeV resonance were also measured. The Ta/N stoichiometry was measured by Rutherford backscattering. Gamma rays were detected using a 135% HPGe detector placed at 0° close to the target. The energy calibration and the absolute photopeak efficiency were obtained using radioactive sources and the decays from well-known resonances in several capture reactions. An important quantity that allows to correct for summing of coincidence γ rays in the HPGe detector is its total efficiency. The latter quantity was calculated using numerical codes and normalized to source data. Finally, a large long-annulus NaI detector enclosing both the target and the germanium crystal, was used as a cosmic-ray veto while also suppressing events arising from γ -ray cascades. Data for different $^{14}\text{N}(p,\gamma)^{15}\text{O}$ transitions were obtained, whereas in Fig. 7 only the results for the transition to the ^{15}O ground state are shown.

The $^{18}\text{F}(p,\alpha)^{15}\text{O}$ Reaction and γ -ray Emission from Novae

Gamma-ray emission from novae is dominated by positron annihilation following β decay of radioactive nuclei [59]. The principal contribution to this emission comes from the decay of newly synthesized ^{18}F and it is therefore of great importance to understand the production and destruction rates of ^{18}F . Moreover, the relatively long half-life of ^{18}F (110 min) means that this annihilation radiation will be present after the expanding envelope of the nova becomes transparent. For this reason, measurements of the ^{18}F abundance are amongst the principal objectives of current and planned γ -ray observatories. The destruction of ^{18}F is determined by the rates of the proton capture reactions $^{18}\text{F}(p,\alpha)^{15}\text{O}$ and $^{18}\text{F}(p,\gamma)^{19}\text{Ne}$, at astrophysically relevant temperatures of 0.1–0.4 GK. The $^{18}\text{F}(p,\alpha)^{15}\text{O}$ reaction is dominant. At these temperatures, properties of states of ^{19}Ne in the vicinity of the $^{18}\text{F}+p$ threshold determine the astrophysical S -factor and therefore the ^{18}F destruction rate. Despite an extensive series of measurements of (p,p) [110–113] and (p, α) [111, 113–117] reactions using radioactive ^{18}F beams, and transfer reactions

to populate states in ^{19}Ne and ^{19}F [90–93, 118–120], significant uncertainties remain, particularly concerning states near the $^{18}\text{F}+p$ threshold.

The direct measurement of $^{18}\text{F}(p,\alpha)^{15}\text{O}$ reaction at the energies corresponding to nova temperature (centre-of-mass energies of about 0.2 MeV) requires a ^{18}F beam of less than 4 MeV with an intensity of at least 10^{12} s^{-1} on target, which is a million times more than the one achievable at present. To overcome the technical difficulty of the direct measurement, indirect methods have been applied, for example, the $^{18}\text{F}(d,p)^{19}\text{F}(\alpha)^{15}\text{N}$ reaction transfer [90–93]. The aim of these measurements was to determine neutron spectroscopic factors for states in ^{19}F that are mirrors to ^{19}Ne states important for the $^{18}\text{F}(p,\alpha)^{15}\text{O}$ reaction. Under the assumption of mirror symmetry, these spectroscopic factor can constrain the rate of the $^{18}\text{F}(p,\alpha)^{15}\text{O}$ reaction. In the Louvain-la-Neuve experiment [90, 91], a 14-MeV ^{18}F radioactive beam of about $2 \times 10^6\text{ s}^{-1}$ bombarded a CD_2 target. Two LEDA silicon strip detector arrays were used to detect protons in coincidence with α particles or ^{15}N ions from the breakup of α -unbound states in ^{19}F . Differential cross sections for the $^{18}\text{F}(d,p)^{19}\text{F}$ reaction were fit by theoretical DWBA distributions to extract neutron spectroscopic factors for excited states in ^{19}F . A similar approach was used in the HRIBF measurement [92, 93], except that better energy resolution was achieved by using a higher bombarding energy (108 MeV). Cross sections for transfer to bound states (with well-known excitation energies) were also measured by detecting ^{19}F ions in the daresbury recoil separator. Figure 8 schematically shows the experimental setup used at HRIBF.

Spectroscopic factors extracted from both of these measurements are consistent and place important new limits on contributions of low-energy resonances to the rate of the $^{18}\text{F}(p,\alpha)^{15}\text{O}$ reaction. Although the uncertainty was considerably reduced, the reaction rates at nova temperatures are still largely uncertain. Figure 9 shows the present S -factor estimates at nova temperatures. The main uncertainties arise from the unknown interference signs between the several $3/2^+$ states near the $^{18}\text{F}+p$ threshold.

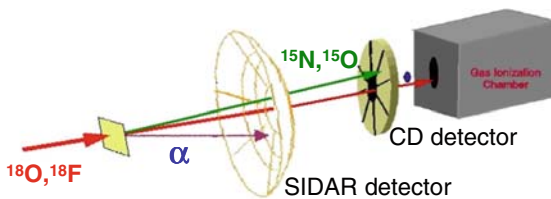


Fig. 8. Experimental setup used at HRIBF to study the $^{18}\text{F}(d,p)^{19}\text{F}(\alpha)^{15}\text{N}$ reaction [92, 93]. The SIDAR and the CD detectors are composed of independent sixteen-strip silicon sectors (See also Plate 32 in the Color Plate Section)

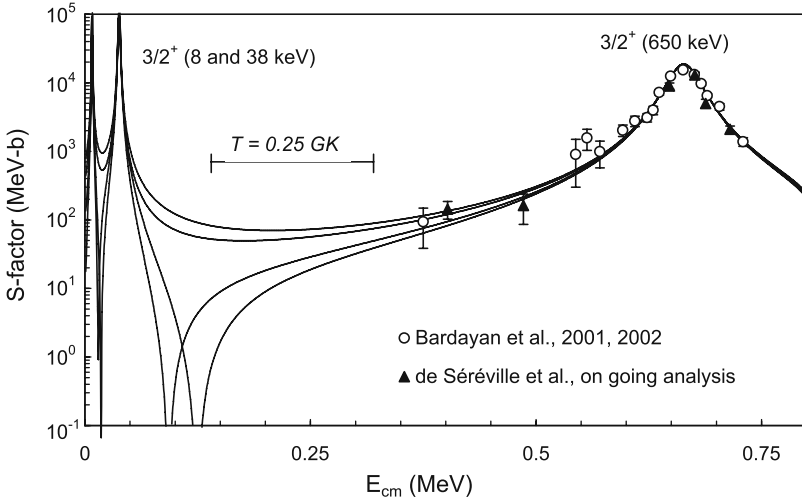


Fig. 9. Astrophysical S -factor of the $^{18}\text{F}(p,\alpha)^{15}\text{O}$ reaction. The curves are R -matrix calculations (for a channel radius $a = 5.5$ fm) using different interference sign for the three $3/2^+$ states situated at 8, 38 and 650 keV above threshold. The Gamow window window for a typical nova temperature of 0.25 GK is indicated. The data are from [111, 117] (*open circles*) and some preliminary results from a recent experiment at Louvain-la-Neuve (*triangles*)

The $^7\text{Be}(d,p)^8\text{Be}$ Reaction and the Primordial ^7Li Problem

The reaction $^7\text{Be}(d,p)^8\text{Be}$, one of the destruction channels of ^7Be (in competition with the electronic capture $^7\text{Be}(e^-\nu)^7\text{Li}$) is related to primordial ^7Li abundance. At present, there is a large difference (about a factor of 2–3) between the ^7Li abundances obtained from nucleosynthesis calculations using reaction rates [28, 31] and the ^7Li abundances observed in halo stars of the Galaxy [121], if one considers the very precise value of the baryonic content of the Universe, $\Omega_b h^2 = 0.0224 \pm 0.0009$,⁶ recently obtained by WMAP [122].

Before suggesting that new physics may be needed to solve this puzzle, effects related to uncertainties in reaction rates involved in the Big Bang nucleosynthesis (BBN) have to be excluded. For high-baryon density, the ^7Li abundance from BBN models arises principally from ^7Be that further decays to ^7Li . Hence reconciliation of BBN, WMAP and ^7Li observations by nuclear physics effects can only come from ^7Be production and destruction rates. In BBN, the main reactions are $^3\text{He}(\alpha,\gamma)^7\text{Be}$ and $^7\text{Be}(n,p)^7\text{Li}$ which are sufficiently well known [31] to exclude this option. However, other reactions have to be considered.

⁶ Ω_b is the ratio of the baryonic density to the critical density, h is the Hubble constant in units of $100 \text{ km s}^{-1} \cdot \text{Mpc}^{-1}$

This is the case of ${}^7\text{Be}(d,p)2\alpha$ reaction. Its reaction rate came from an estimate by Parker [123] based on partial experimental data above the centre-of-mass energy of 0.6 MeV from an early work of Kavanagh [124]. In [124], protons corresponding to the 0^+ ground state and the first excited state (3.06 MeV, 2^+) in ${}^8\text{Be}$ were detected at 90° using a NaI(Tl) detector. The estimate of the ${}^7\text{Be}(d,p)2\alpha$ cross sections at the Gamow window ($T = 0.1 - 1$ GK, $E = 0.11 - 0.56$ MeV) implies an extrapolation of about two orders of magnitude. If the actual ${}^7\text{Be}(d,p)2\alpha$ reaction rate were a factor of about 100 larger at these low energies, where no data existed, the ${}^7\text{Li}$ disagreement would vanish. Figure 10 shows the level scheme of ${}^9\text{B}$ and ${}^8\text{Be}$, and the ${}^7\text{Be}(d,p)2\alpha$ reaction threshold ($Q = 16.490$ MeV) [125]. In addition to the ground state and the first excited state in ${}^8\text{Be}$, investigated so far [124], higher-lying states in ${}^8\text{Be}$ can have a non-negligible contribution to the ${}^7\text{Be}(d,p)2\alpha$ reaction cross section. This reaction has been recently investigated using a radioactive ${}^7\text{Be}$ beam at c.m. energies $E = 0.96 - 1.2$ MeV ($E_{\text{lab}} = 5.55$ MeV) and $E = 0.15 - 0.38$ MeV ($E_{\text{lab}} = 1.71$ MeV) and a $200 \mu\text{g}/\text{cm}^2$ $(\text{CD}_2)_n$ target [126].

Because of the high Q -value, the expected laboratory energies of the reaction products (protons, α -particles, ...) are high and thus particle identification is needed, e.g. by using a ΔE - E telescope. For example, protons produced by an incoming 5.55 MeV ${}^7\text{Be}$ beam over the target thickness, and feeding all ${}^8\text{Be}$ states below the ${}^7\text{Be}+d$ threshold, have energies ranging from 2.5 to 22 MeV for the covered angles. Hence, to distinguish the protons coming from the ${}^7\text{Be}+d$ reaction from those arising from reactions on the carbon content of the target, a stack of two silicon strip detector LEDA arrays [65] were used. They covered laboratory angles from 7.6° to 17.4° . Two energy-loss measurements were performed by detector arrays abbreviated as ΔE_1 and ΔE_2 . The former consisted of eight detectors of 0.3 mm thickness, while the latter included four of 0.3 mm and four of 0.5 mm thickness. Alpha particles, recoil and scattered particles from ${}^7\text{Be}+{}^{12}\text{C}$ reactions were completely stopped in ΔE_1 . From all the open reaction channels, only protons from the ${}^7\text{Be}+d$ reaction were able to pass through both ΔE_1 and ΔE_2 detector arrays. High-energy protons corresponding to the ground state and the first excited state in ${}^8\text{Be}$ were not completely stopped in the $\Delta E_1 - \Delta E_2$ telescope, while protons corresponding to other higher-lying excited states in ${}^8\text{Be}$ were stopped in ΔE_2 .

Figure 11 shows a typical $\Delta E_1 - \Delta E_2$ calibrated spectrum obtained at ${}^7\text{Be}$ beam energies of 5.55 MeV. This spectrum corresponds to the total number of counts integrated in the entire detector [126]. The proton signals are well separated from the uncorrelated background ($\Delta E_2 < 1$ MeV). The most strongly populated regions correspond to the feeding of the 0^+ ground state and 2^+ excited state in ${}^8\text{Be}$. The two levels are unresolved. The two cluster of events observed are due to the different silicon wafer thicknesses (0.3 and 0.5 mm, respectively) used for ΔE_2 . The regions of interest were calculated by taking into account the kinematics of the reaction populating these states, the width of the states, the straggling of the beam in the target, and the energy loss

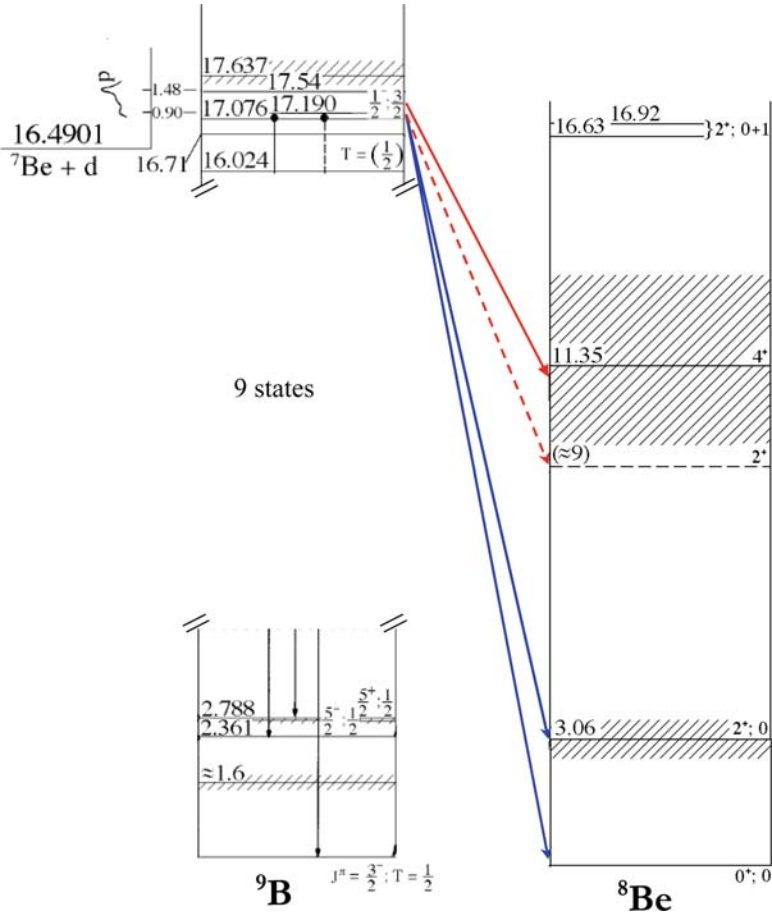


Fig. 10. ${}^9\text{B}$ and ${}^8\text{Be}$ level scheme [125]. The (d,p) reactions populating the ground state and first excited state of ${}^8\text{Be}$ were investigated by Kavanagh [124]. Other ${}^8\text{Be}$ states of interest are also indicated (See also Plate 33 in the Color Plate Section)

of protons in ΔE_1 and ΔE_2 [127]. Other events correspond to the feeding of the higher-lying ${}^8\text{Be}$ levels for which part of the protons are stopped in ΔE_2 , hence characterized by a different shape in the $\Delta E_1 - \Delta E_2$ plot.

Figure 12 shows the results as the ${}^7\text{Be}(d,p)2\alpha$ reaction astrophysical S -factor. The full triangles are the contribution from the ground state and the first excited state in ${}^8\text{Be}$ (about 65% of the total), in good agreement with the data from [124] (open circles). The full circles include the contribution of a large 4^+ state at 11.35 MeV in ${}^8\text{Be}$ (see Fig. 10). These results show that the states not observed by [124] account for about 35% of the total S -factor and not of a factor of 3 as previously estimated [123]. This means that the

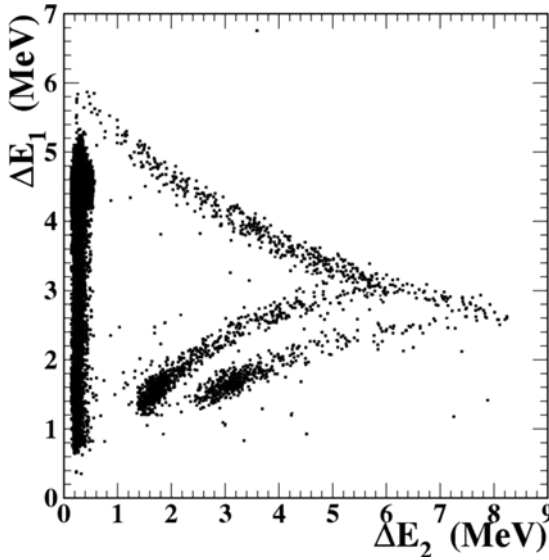


Fig. 11. Typical $\Delta E_1 - \Delta E_2$ proton spectrum obtained for a ${}^7\text{Be}$ beam energy of 5.55 MeV and a 200 μm thick $(\text{CD}_2)_n$ target [126]. See text for details

${}^7\text{Be}(d,p)2\alpha$ reaction cross section is about ten times smaller than previously estimated at Big Bang energies, thus excluding a solution via nuclear physics of the primordial ${}^7\text{Li}$ problem.

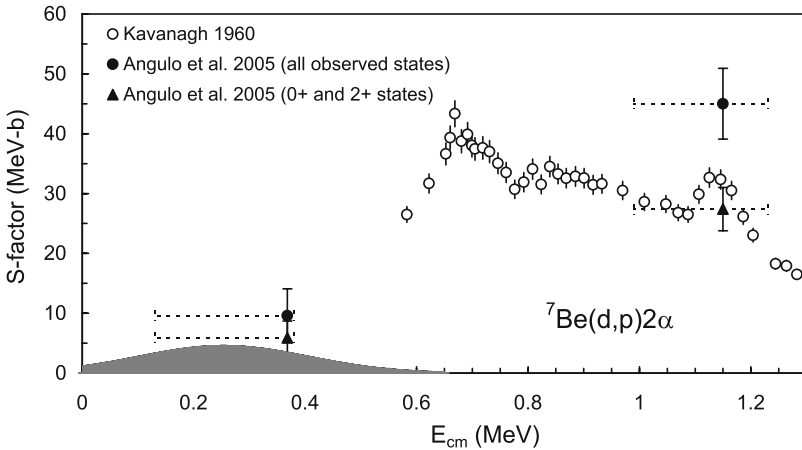


Fig. 12. Astrophysical S -factor of ${}^7\text{Be}(d,p)2\alpha$ reaction [126]. The Gamow peak for a typical Big Bang temperature of 0.8 GK is shown in grey

5 Future Challenges and Conclusions

The understanding of stellar burning confronts physicists with many challenges across a wide range of nuclear physics topics, the corresponding experimental programs being characterized by many technical difficulties. After more than 30 years of research using stable-isotope beams, there are still reactions involved in quiescent burning whose cross sections are unknown in the energy range of interest and, consequently, the astrophysical predictions are still too uncertain for stellar systems that are, in principle, not very exotic, like the sun. Background sources in the laboratory are the main challenge for such measurements. Underground facilities seems to offer a solution to overcome the experimental difficulties, although they face other technical problems.

Our understanding of the energy source and nucleosynthesis in explosive events is reflected in our knowledge of the properties of the related unstable nuclei and the reaction rates involving them. Since about one decade, the development of radioactive beams has made it possible to investigate some reactions involved in such explosive events. Experimental approaches used traditionally with stable-isotope beams (elastic and inelastic scattering, transfer reactions) have been successfully used to obtain information on the properties of astrophysically important states of some radioactive nuclei. Indirect technique using, e.g., transfer reactions are particularly appealing for measurements with low-intensity radioactive beams. However, such approaches are model-dependent, and uncertainties related to the model will be reflected in the results. In spite of the progress, many key reactions and key quantities, which are the most challenging ones, remain largely unknown. This is specially true for the r -process path. More intense and new radioactive beams and sophisticated detection systems are therefore required. On the other hand, nuclear theory must be exploited to avoid misinterpretation of experimental data and a close collaboration with astronomical observations and astrophysical modelling is as essential as ever.

Acknowledgement

The author thanks Ernst Roeckl and Jim Al-Khalili for constructive comments and a careful reading of the manuscript. This work is supported by the European Commission within the Sixth Framework Programme through I3-EURONS (contract no. RII3-CT-2004-506065).

References

1. G. Wallerstein et al.: Rev. Mod. Phys. **69**, 995 (1997) 253
2. K. Käppeler, F.-K. Thielemann, M. Wiescher: Ann. Rev. Nucl. Part. Sc. **48**, 175 (1998)

3. M. Arnould, T. Takahashi: Rep. Prog. Phys. **62**, 393 (1999)
4. K. Käppeler: Prog. Part. Nucl. Phys. **43**, 419 (1999) 256
5. Langanke, K., Thielemann, K.-F., Wiecher, M.: Nuclear astrophysics and nuclear far from stability. In: Al-Khalili, J.S., Roeckl E. (eds.) Lecture Notes in Physics, Vol. 651, pp. 383–467. Springer, Heidelberg (2004) 253
6. D.D. Clayton: *Principles of stellar evolution and nucleosynthesis*, 2nd edn. (University of Chicago Press, 1968) 253, 254, 256, 257, 258, 260, 261, 262
7. H.A. Bethe, C.L. Critchfield: Phys. Rev. **54**, 248 (1938) 254
8. H.A. Bethe: Phys. Rev. **55**, 434 (1939)
9. H.A. Bethe: Science **161**, 541 (1968) (Nobel Lecture). 254
10. F. Hoyle: Mon. Not. R. Astron. Soc. **106**, 343 (1946) 254
11. E.M. Burbidge, G.R. Burbidge, W.A. Fowler, F. Hoyle: Rev. Mod. Phys. **29**, 547 (1957) 254
12. C. Angulo: Contributions récents à l'astrophysique nucléaire. Habilitation Thesis, Université catholique de Louvain, Louvain-la-Neuve (2006). 255, 263, 273
13. C. Iliadis: *Nuclear Physics of Stars* (Wiley-VCH Verlag GmbH, 2007) 254, 258, 260, 261
14. C. Angulo: 'Experimental approach to nuclear reactions of astrophysical interest involving radioactive nuclei'. In: *Exotic Nuclei and Nuclear/Particle Astrophysics, Carpathian Summer School of Physics 2005 at Mamaia, Constanta, Romania, June 13–24, 2005*, ed. by S. Stoica, L. Trache, R.E. Tribble (World Scientific, Singapore 2006) pp. 264–266 255
15. C. Angulo et al.: Nucl. Phys. A **656**, 3 (1999) 255, 257, 259, 260, 261, 272
16. J.C. Blackmon, C. Angulo, A.C. Shotton: Nucl. Phys. A **777**, 531 (2006) 255, 256, 264
17. Huysse, M.: The why and how of radioactive-beam research. In: Al-Khalili, J.S., Roeckl E. (eds.) Lecture Notes in Physics, Vol. 651, pp. 1–32. Springer, Heidelberg (2004). 256, 262
18. P. Descouvemont: *Theoretical Models in Nuclear Astrophysics* (Nova Science Publishers Inc., New York 2003) 256, 258, 259
19. M.S. Smith, K.E. Rehm: Annu. Rev. Nucl. Part. Sci. **51**, 91 (2001) 256
20. S. Kubono: Nucl. Phys. A **693**, 221 (2001) 256
21. E.E. Salpeter: Phys. Rev. **88**, 547 (1952) 257
22. R. Bonetti et al.: Phys. Rev. Lett. **82**, 5205 (1999) 257, 258, 264
23. P. Descouvemont, D. Baye, P.-H. Heenen: Z. Phys. A **306**, 79 (1982) 258
24. C. Arpesella et al.: Phys. Lett. B **389**, 452 (1996) 258
25. M. Junker et al.: Phys. Rev. C **57**, 2700 (1998) 258
26. P. Descouvemont: Phys. Rev. C **70**, 065802 (2004) 259
27. J.N. Bahcall, M.H. Pisonneault: Phys. Rev. Lett. **92**, 121301 (2004) 260, 271, 273
28. A. Coc et al: Astrophys. J. **600**, 544 (2004) 260, 275
29. B.S. Nara Singh et al.: Phys. Rev. Lett. **93**, 262503 (2004) 262503. 260
30. D. Bemmerer et al.: Phys. Rev. Lett. **97**, 122502 (2006) 260
31. P. Descouvemont et al.: At. Data Nucl. Data Tables **88**, 203 (2004) 260, 275
32. P.A. Bergbusch, B.A. Vanderberg: Astrophys. J. Suppl. **81**, 163 (1992) 260, 271
33. B. Chaboyer et al.: Science **271**, 957 (1996)
34. B. Chaboyer et al.: Astrophys. J. **494**, 96 (1998) 260, 271
35. R. C. Runkle et al.: Phys. Rev. Lett. **94**, 082503 (2005) 260, 272, 273
36. F. Herwig, S.M. Austin, J.C. Lattanzio: Phys. Rev. C **73**, 025802 (2006) 260, 261
37. A. Formicola et al.: Phys. Lett. B **591**, 61 (2004) 260, 264, 271, 272
38. C.W. Cook, W.A. Fowler, C.C. Lauritsen, T. Lauritsen: Phys. Rev. **107**, 508 (1957) 261

39. C.W. Cook, W.A. Fowler, C.C. Lauritsen, T. Lauritsen: Phys. Rev. **111**, 567 (1958) 261
40. H.O.U. Fynbo et al.: Nature **433**, 136 (2005) 261
41. L.R. Buchmann, C.A. Barnes: Nucl. Phys. A **777**, 254 (2006) 261
42. R. Gallino et al.: Astrophys. J. **497**, 388 (1998) 261
43. C.R. Brune, I. Licot, R.W. Kavanagh: Phys. Rev. C **48**, 3119 (1993) 261
44. H.W. Drotleff et al.: Astrophys. J. **414**, 735 (1993) 261
45. P. Descouvemont: Phys. Rev. C **36**, 2206 (1987) 261
46. J. José, A. Coc: 'Nucleosynthesis in Classical Nova Explosions: Modeling and Nuclear Uncertainties'. In: *Nuclear Physics News International*, Vol. 15, No. 4 (2005) p17. 261
47. H. Schatz et al.: Astrophys. J. **524**, 1014 (1999) 262
48. H. Schatz et al.: Nucl. Phys. A **688**, 150 (2001) 262
49. J. José: Nucl. Phys. A **752**, 540c (2005) 262
50. C. Fox et al.: Phys. Rev. Lett. **93**, 081102 (2004) 262
51. C. Fox et al.: Phys. Rev. C **71**, 055801 (2005)
52. A. Chafa et al.: Phys. Rev. Lett. **95**, 031101 (2005); Erratum: Phys. Rev. Lett. **96**, 0199902 (2006) 262
53. S. Bishop et al.: Phys. Rev. Lett. **90**, 162501 (2003); Erratum: Phys. Rev. Lett. **90**, 229902 (2003) 262
54. B. Davids et al.: Phys. Rev. C **68**, 055805 (2003)
55. J.M. D'Auria et al.: Phys. Rev. C **69**, 065803 (2004) 262
56. D.G. Jenkins et al.: Phys. Rev. Lett. **92**, 031101 (2004) 262
57. S.E. Hale et al.: Phys. Rev. C **70**, 045802 (2004) 262
58. D.G. Jenkins et al.: Phys. Rev. C **72**, 031303 (2005) 262
59. A. Coc, M. Hernánz, J. José J.-P. Thibaud: Astron. Astrophys. **357**, 561 (2000). 262, 273
60. W. Galster et al.: Phys. Rev. C **44**, 2776 (1991) 263
61. K.E. Rehm et al.: Nucl. Instr. and Meth. in Phys. Res. **449**, 208 (1998) 263, 266
62. F. Vanderbist et al.: Nucl. Instr. and Meth. in Phys. Res. B **197**, 165 (2002) 263
63. D.A. Hutcheon et al.: Nucl. Instr. and Meth. in Phys. Res. A **498**, 190 (2003) 264, 266
64. G. Fiorentini, R.W. Kavanagh, C. Rolfs: Z. Phys. A **350**, 289 (1995) 264
65. T. Davinson et al.: Nucl. Instr. and Meth. in Phys. Res. A **454**, 350 (2000) 264, 265, 269
66. C. Angulo et al.: Nucl. Phys. A **716**, 213 (2003) 265, 268
67. I.Y. Lee: Nucl. Phys. A **520**, 641c (1990) 265
68. C.N. Davids: Nucl. Instr. and Meth. in Phys. Res. B **204**, 124 (2003) 266
69. D. Schürman et al.: Nucl. Instr. and Meth. in Phys. Res. A **531**, 428 (2004). 266
70. R. Fitzgerald et al.: Nucl. Phys. A **748**, 351 (2005). 266
71. J. Görres: Proceedings of Science, (NIC-IX) 027. 266
72. D. Lunney, J.M. Pearson, C. Thibault: Rev. Mod. Phys. **75**, 1021 (2003) 267
73. Ultra-accurate mass spectrometry and related topics, Jürgen Kluge Special Issue, Intl. J Mass Spectrom. **251**, 85 (2006)
74. K. Blaum: Phys. Rep. **425**, 1 (2006) 267
75. R.A. Laubenstein et al.: Phys. Rev. **84**, 12 (1951) 267
76. K.P. Artemov et al.: Yad. Fiz. **52**, 634 (1990) [Sov. J. Nucl. Phys. **52**, 408 (1990)] 267
77. Th. Delbar et al.: Nucl. Phys. A **542**, 263 (1992) 267
78. A.M. Lane, R.G. Thomas: Rev. Mod. Phys. **30**, 257 (1958) 268
79. G.V. Rogachev et al.: Phys. Rev. C **64**, 061601 (2001) 268
80. C. Angulo et al.: Phys. Rev. C. **67**, 014303 (2003), and references therein

81. C. Angulo: Nucl. Phys. A **746**, 222c (2004) 268
82. C. Ruiz et al.: Phys. Rev. C **65**, 042801 (2002) 269
83. J. D'Auria et al.: Phys. Rev. C **69**, 065803 (2004) 269
84. B. Harss et al.: Phys. Rev. Lett. **82**, 3964 (1999) 269
85. J.C. Blackmon et al.: Nucl. Phys. A **688**, 142c (2001) 269
86. B. Harss et al.: Phys. Rev. C **65**, 035803 (2002) 269
87. J.C. Blackmon et al.: Nucl. Phys. A **718**, 127c (2003) 269
88. G.R. Satchler: *Direct Nuclear Reactions* (Clarendon Press, Oxford, 1983) 270
89. K.E. Rehm et al.: Phys. Rev. Lett. **80**, 676 (1998) 270
90. N. de Séréville et al.: Phys. Rev. C **67**, 052801 (2003) 270, 274
91. N. de Séréville et al.: submitted to Phys. Rev. C 270, 274
92. R.L. Kozub et al.: Phys. Rev. C **71**, 032801 (2005) 270, 274
93. R.L. Kozub et al.: Phys. Rev. C **73**, 044307 (2006) 270, 274
94. R.A. Paddock: Phys. Rev. C **5**, 485 (1972) 270
95. D.R. Osgood, J.R. Patterson, E.W. Titterton: Nucl. Phys. **60**, 503 (1964) 270
96. K.I. Hahn et al.: Phys. Rev. C **54**, 1999 (1996) 270
97. R. Mendelson, G.J. Wozniak, A.D. Bacher, J.M. Loiseaux, J. Cerny: Phys. Rev. Lett. **25**, 533 (1970) 270
98. J.A. Caggiano et al.: Phys. Rev. C **66**, 015804 (2002) 270
99. Y. Parpottas et al., Phys. Rev. C **70**, 065805 (2004); Erratum: Phys. Rev. C **73**, 049907 (2006) 270
100. W. Benenson et al.: Phys. Rev. C **15**, 1187 (1977) 270
101. H. Schatz et al.: Phys. Rev. Lett. **79**, 3845 (1997) 3845 270
102. M. Wiescher et al.: Nucl. Phys. A **484**, 90 (1988) 270
103. J.A. Caggiano et al.: Phys. Rev. C **64** 025802 (2001) 270
104. J.A. Caggiano et al.: Phys. Rev. C **65** 055801 (2002) 270
105. U. Schröder et al.: Nucl. Phys. A **467**, 240 (1987) 272
106. C. Angulo, P. Descouvemont: Nucl. Phys. A **690**, 755 (2001) 272
107. P.F. Bertone et al.: Phys. Rev. Lett. **87**, 152501 (2001) 272
108. K. Yamada et al.: Phys. Lett. B **579**, 265 (2004) 272
109. C. Angulo, A.E. Champagne, H.P. Trautvetter: Nucl. Phys. A **758**, 391c (2005) 272
110. D.W. Bardayan et al.: Phys. Rev. C **62**, 042802 (2000) 273
111. D.W. Bardayan, et al.: Phys. Rev. C **63**, 065802 (2001) 273, 275
112. D.W. Bardayan et al.: Phys. Rev. C **70**, 015804 (2004)
113. J.-S. Graulich et al.: Phys. Rev. C **63**, 011302 (2001) 273
114. R. Coszach et al.: Phys. Lett. B **353** 184 (1995)
115. K.E. Rehm et al: Phys. Rev. C **52**, 460 (1995)
116. J.S.Graulich et al.: Nucl. Phys. A **626**, 751 (1997)
117. D.W. Bardayan et al.: Phys. Rev. Lett. **89**, 262501 (2002) 273, 275
118. F. de Oliveira et al.: Phys. Rev. C **55**, 3149 (1997) 274
119. S. Utku et al.: Phys. Rev. C **57**, 2731 (1998), Erratum: Phys. Rev. C **58**, 1354 (1998)
120. D.W. Visser et al.: Phys. Rev. C **69**, 048801 (2004) 274
121. S.G. Ryan et al.: Astrophys. J. **530**, L57 (2000) 275
122. D.N. Spergel et al.: Astrophys. J. Suppl. **148**, 175 (2003) 275
123. P.D. Parker: Astrophys. J. **175**, 261 (1972) 276, 277
124. R.W. Kavanagh: Nucl. Phys. **18**, 492 (1960) 276, 277
125. F. Ajzenberg-Selove: Nucl. Phys. A **490**, 1 (1988) 276, 277
126. C. Angulo et al.: Astrophys. J. **630**, L105 (2005) 276, 278
127. J.F. Ziegler, J.P. Biersack: SRIM program, v2003.26. 277